# Subclonal evolution and expansion of THY1-positive cells is associated with recurrence in glioblastoma

**Authors:** Wajd N. Al-Holou[1]†, Hanxiao Wang[2,5]†, Visweswaran Ravikumar[4], Morgan Oneka[4], Roel GW Verhaak[7], Hoon Kim[7], Drew Pratt[3], Sandra Camelo-Piragua[3], Corey Speers[2], Todd Hollon[1], Oren Sagher[1], Jason A Heth[1], Karin M. Muraszko[1], Theodore S. Lawrence[2], Ana C de Carvalho[6], Tom Mikkelsen[6], Arvind Rao[2,4], Alnawaz Rehemtulla[2*]

**Affiliations:**

[1]Department of Neurosurgery, The University of Michigan Medical School; Ann Arbor, MI 48109.

[2]Department of Radiation Oncology, The University of Michigan Medical School; Ann Arbor, MI 48109.

[3]Department of Pathology, The University of Michigan Medical School; Ann Arbor, MI 48109.

[4] Department of Computational Medicine & Bioinformatics, The University of Michigan Medical School; Ann Arbor, MI 48109.

[5] AstraZeneca.

[6] Department of Neurosurgery, Henry Ford Hospital; Detroit, MI 48202.

[7] The Jackson Laboratory; Farmington, CT 06032.

*Corresponding author. Alnawaz Rehemtulla, University of Michigan, NCRC 520, Room 1342 Ann Arbor, MI 48105, Email: alnawaz@med.umich.edu

**One Sentence Summary:** THY1 positive tumor cells drive resistance in glioblastoma

**Abstract:** Glioblastoma(GBM) is a lethal disease characterized by treatment resistance and recurrence. To investigate the mechanisms that drive treatment resistance in GBM, we developed a longitudinal *in vivo* recurrence model utilizing patient-derived GBM explants to produce paired specimens pre- and post-recurrence following temozolomide(TMZ) and radiation(IR) therapy. These studies revealed in replicate cohorts, a common gene expression profile upon recurrence, characterized by an upregulation of transcripts associated with a mesenchymal and stem cell phenotype, including *TGFβ1, TGFβ2, SOX2, ZEB2, GLI2* and *THY1(CD90),* with greater than one-hundred-fold increase in *THY1* levels. Analyses of clinical databases revealed the association of this transcriptional profile with worse overall survival and elevation in recurrent tumors. We then isolated THY1-positive cells from treatment-naïve patient samples which demonstrated inherent resistance to chemoradiation when implanted intracranially. Additionally, using image-guided biopsies from treatment-naïve human GBM we conducted spatial whole transcriptomic analyses. This revealed rare *THY1*+ regions characterized by elevation of the mesenchymal and stem-like gene expression profile, previously identified in our *in vivo* recurrent samples, which co-localized with a macrophage gene signature within the perivascular niche. Since TGFβ signaling contributes to a mesenchymal/stem-like phenotype and therapeutic resistance, and to investigate its effect on THY1, we inhibited TGFβRI kinase activity *in vivo* which resulted in decreased expression of genes characteristic of a mesenchymal/stem-like phenotype, including THY1. Notably, TGFβRI inhibition restored sensitivity to TMZ/IR in recurrent tumors *in vivo*. These studies reveal that post-TMZ/IR recurrence may result from tumor repopulation by pre-existing, therapy-resistant, THY1-positive mesenchymal/stem-like cells within the perivascular niche.

## INTRODUCTION

Glioblastoma(GBM), the most common primary intraparenchymal brain tumor, is a lethal disease with a median survival of 15 months that is characterized by treatment resistance, aggressive brain invasion, and inevitable recurrence, with less than 10% of patients surviving beyond 5 years(*1, 2*). A major obstacle contributing to rapid recurrence and the lack of effective treatments is the marked intra- and inter-tumoral heterogeneity in GBM(*3-6*). Furthermore, given the heterogeneity present within GBM, it has been postulated that evolution and expansion of pre-existing treatment-resistant sub-clones are often responsible for inevitable recurrence (*5, 7, 8*). Intratumoral heterogeneity can be seen at both at the cellular and microenvironmental level. At the tumor microenvironmental level, distinct niches, especially perivascular, hypoxic, and invasive tumor niches, have been shown to be enriched with therapy-resistant cancer stem cell(CSC) populations, also described as recurrence-initiating stem cells (*3, 7, 9*). These pre-existing CSC populations are thought to play a critical role in driving treatment resistance and are characterized by self-renewal, differentiation, and the ability to expand and repopulate tumors post-therapy(*10*). Definitive evidence for the role for pre-existing treatment-resistant cancer stem cells in evading chemo-radiation therapy as well as the mechanistic basis for this phenotype is lacking. An understanding of the genetic basis for the therapy resistant phenotype should provide an opportunity for therapeutic intervention to decrease the recurrence rate in GBM.

In this effort, we have utilized a longitudinal mouse model developed using patient-derived GBM explants to recapitulate the clinical treatment paradigm. Using this model, we generated pre-treatment and recurrent paired samples from each experimental mouse with the goal of identifying differentially expressed genes that should provide a molecular basis for tumor

recurrence. Systematic analyses of multiple replicate intracranial patient-derived xenografts(PDX) revealed that recurrent tumors were characterized by a gene expression pattern characteristic of a mesenchymal and CSC signature, which include upregulation of *THY1/CD90, TGFβ1, TGFβ2, SOX2, ZEB2, and GLI2*. Consistent with previous observations, we demonstrate using a large GBM cohort that this gene expression profile is associated with a worse overall prognosis, highlighting the clinical implications of our findings. To test the hypothesis that tumor recurrence may be attributed to a pre-existing cell population characterized by this gene expression signature, we immuno-sorted THY1+ cells from treatment-naïve patient samples and demonstrated that intracranial tumors derived from THY1+ cells (Pre-THY1+) were inherently treatment resistant compared to unsorted tumors. These results suggest that rare populations of inherently treatment-resistant cells with distinct gene expression profiles can be found within the original treatment-naïve tumors, and are responsible for tumor recurrence(*5, 8, 11*). In support, treatment of tumors with a targeted agent that reverses the mesenchymal gene expression signature, resulted in restoration of sensitivity to chemoradiation therapy. Furthermore, spatial transcriptomic analyses of human GBM specimens consistently identified *THY1*+ cells co-localized with expression of mesenchymal, glioma stem cell, and macrophage gene signatures and were primarily found within a perivascular niche. This suggests an important role for these rare resistant cells in the vascular tumor micro-environment.

## RESULTS

### *in vivo* modeling reveals initial therapeutic response to TMZ/IR followed by recurrence

To evaluate the therapeutic response and the underlying genetic basis for resistance to standard of care therapy (TMZ/IR) in GBM, we utilized patient derived explants in intracranial xenografts (Fig. 1). Magnetic resonance imaging was performed weekly to monitor tumor

growth after implantation. Mice bearing tumors of approximately 20mm$^3$ were randomized into three study cohorts. The first represented control untreated animals, and a second was treated with concurrent TMZ/IR for two weeks. A third cohort was administered concurrent TMZ/IR for 2 weeks followed by adjuvant TMZ three times a week, every other week after completion of the second week of TMZ/IR. This experimental design was intended to investigate mechanisms of resistance to standard of care therapy (Fig. 1A). In contrast to control animals which exhibited a greater than 300% increase in tumor volume and succumbed to disease by the third week, TMZ/IR treated animals exhibited an initial tumor regression and survived beyond six weeks. Mice that received adjuvant TMZ exhibited a greater delay in tumor growth and had a prolonged survival (>12 weeks). Despite an initial response to therapy, all treated animals had recurrence (Fig. 1B and 1C).

To better understand the underlying genetic basis for the development of therapeutic resistance, an MRI-guided stereotactic intracranial biopsy was used to obtain tumor tissue from selected animals prior to initiation of treatment. This biopsy procedure does not significantly impact the gross tumor architecture(*12*)(Fig. S1). Viable tumor tissue was also obtained from these animals upon recurrence. The paired pre-treatment and recurrent tumor samples were collected for further analyses.

**Recurrent tumors are distinctly resistant to TMZ/IR**

To evaluate the sensitivity of recurrent tumors to therapy, paired neurosphere cultures derived from pre-treatment and recurrent biopsies were implanted intracranially and subcutaneously into immune-deficient mice. Subcutaneously implanted murine models with palpable tumors were randomized into a control group or treated with TMZ/IR for two weeks followed by adjuvant TMZ as above. In the absence of treatment, pre-treatment and recurrent

tumors grew at a similar rate. In response to treatment, pre-treatment tumors demonstrated a significant delay in tumor growth (analogous to the initial patient-derived tumors), while tumors derived from recurrent biopsies exhibited resistance to TMZ/IR treatment. Treatment of tumors derived from pre-treatment samples exhibited a 50% decrease in tumor volume while recurrent tumors exhibited a 750% increase in tumor volume(Fig. 1D). To confirm these findings in an appropriate tumor microenvironment, intracranial tumors were established using the same paired neurospheres. Treatment of mice bearing intracranial recurrent tumors with TMZ/IR plus adjuvant TMZ demonstrated their resistance to therapy compared to those derived from pre-treatment samples (Fig. 1E). In support, the median survival of mice bearing recurrent tumors was 7 weeks compared to 11.9 weeks for treatment naïve tumors($p=0.006$) (Fig. 1F).

**Recurrent samples develop a therapeutic resistant phenotype with increased mesenchymal and stem cell gene expression patterns and *THY1* upregulation**

To delineate the underlying genomic basis for the observed resistance to therapy in recurrent samples, the transcriptome of at least three independent replicates of pre-treatment and recurrent biopsies from the same subject animals was evaluated using RNAseq(Fig. 2A). 1159 genes were found to be differentially expressed ($FDR<0.05$). Among these differentially expressed genes, 645 genes were upregulated in recurrent tumor samples while 514 genes were downregulated. Unsupervised clustering analysis showed that each of the independent replicate pre-treatment biopsies and recurrence samples had a similar gene expression pattern but distinct from the pre-treatment samples (Fig. 2B, Fig. S2). Moreover, the transcriptome of each pre-treatment sample closely resembled that of the original patient derived neurosphere cultures, demonstrating that gene expression profile did not drift significantly after *in vitro* expansion or upon intracranial implantation.

We then carried out a Gene Ontology analysis using David to identify common cellular processes that underlie these changes in gene expression. 20 functional clusters within the upregulated genes and 13 functional clusters in downregulated genes were identified (FDR<0.05). Consolidation of clusters having a role in overlapping biological processes yielded 10 upregulated gene clusters and seven downregulated gene clusters (Fig. 2C). Of the seven downregulated clusters, six were associated with apoptosis and cell death. Genes involved in cell adhesion, neuronal differentiation/development, and cellular morphogenesis were dominant in the upregulated clusters. A closer analysis of the upregulated genes within the cell adhesion cluster (Fig. 2D) revealed the presence of a number of genes associated with a role in cell-cell and cell-extra cellular matrix adhesion (e.g. *ITGB3, ITGB5, ITGB8, NEDD9, FBLN7, NLGN2, CADM1 and VCAN*) as well as genes associated with a mesenchymal phenotype (*TGFB2, TGFB1, THY1*).

Upregulation of this gene expression signature was found to be associated with a therapy resistant phenotype as indicated by a worse prognosis in a clinical database. A metagene score was created based on the average gene expression level of the top 64 cell adhesion genes. We selected GBM patients treated with TMZ and IR from the TCGA database and ranked them based on the metagene scores. Overall survival and tumor-progression-free days were evaluated in the patients with a high metagene score (upper 1/3 total selected patients) and those with a low metagene score (lower 1/3 of total selected patients). As shown in Figs. 2E and 2F, patients with a high metagene score had worse clinical outcome, both in terms of median progression free survival (260 days compared to 189 days), as well as median overall survival (median survival of 430 days compared to 248 days) supporting the experimental mouse model derived results that

an increase in the experimentally observed signature correlates with a therapeutic resistance in patients.

To validate findings from the RNAseq differential gene expression studies, we selected genes associated with a cell adhesion, mesenchymal as well as a stem phenotype (*ZEB2, VCAN, CDK6, THY1, GLI2, SOX2*), which have previously been associated with therapeutic resistance in GBM(*13-16*). Quantitative PCR analysis confirmed that *ZEB2, VCAN, CDK6, THY1, GLI2,* and *SOX2* mRNA levels were upregulated in all four recurrent tumor samples compared to their treatment naïve counterparts (Figs. 3A,B). Western blot analysis confirmed that the protein levels for each of these genes were also increased in a majority of recurrent samples compared to their untreated counterparts (Figs. 3C,D). Expression of the CD133 cell surface epitope, a marker of glioma stemness, was also markedly elevated in three of the four recurrent tumors (Fig. 3B).

In contrast to these consistent changes in gene expression observed between replicate recurrent tumors, analysis of copy number gain or copy number loss between each of the pre-treatment and recurrent samples did not show any significant and consistent changes (Fig. S3). This suggests that development of the resistance phenotype resulted from changes in gene expression rather than genomic changes, highlighting the importance of modulation of the relevant cell signaling pathways identified.

**Inhibition of TGFβ signaling decreases *THY1* expression, reverse the mesenchymal resistance phenotype, and results in improved treatment sensitivity *in vivo***

In our recurrent tumors, the resistance phenotype is characterized by increased expression of mesenchymal and CSC genes. Specifically, the TGFβ pathway was also significantly upregulated. In fact, many (21 of 63) of the upregulated genes within the recurrent tumors are

associated directly or indirectly with the TGFβ signaling pathway. TGFβ is considered a master regulator of epithelial to mesenchymal transition. To evaluate the association of TGFβ signaling with the upregulated gene expression profile and to TMZ/IR resistance, we utilized an inhibitor of the TGFβR1 serine threonine kinase. Animals bearing flank tumors derived from pre-treatment (P2) as well as recurrent tumors (R1) were randomized into four groups: 1) Control (untreated), 2) TMZ/IR treatment, 3) Treatment with TGFβ inhibitor alone (LY2109761), and 4) treatment with a combination of TMZ/IR and LY2109761. Western blot analysis of untreated tumor samples (P2 and R1) as well as treated recurrent tumor samples (RT1-5) revealed that treatment of tumors with LY2109761 resulted in decreased levels of THY1, ZEB2, CDK6, SOX2, and GLI2 compared to the untreated recurrent tumors (Fig. 4A). Furthermore, these markers of a mesenchymal/stem phenotype were also downregulated in tumors that received TMZ/IR and concurrent LY2109761.

Evaluation of treatment response revealed that LY2109761 as a single agent did not demonstrate a significant change in tumor growth rate (Fig 4B). Most significantly, treatment of mice bearing recurrent tumors with standard of care TMZ/IR combined with LY2109761 resulted in a substantial decrease in tumor growth compared to single agent LY2109761 or TMZ/IR treatment (Fig. 4B). This indicated that TGFβ inhibition resulted in the downregulation of the mesenchymal and stem-like gene expression profiles, and restored sensitivity to TMZ/IR.

**Rare THY1+ cell populations derived from treatment naive samples are inherently TMZ/IR resistant, and repopulate the recurrent tumors**

The above finding that *THY1* transcript and protein levels were upregulated within the recurrent tumor samples (more than 100-fold compared to treatment-naïve samples, Fig. 3A)

combined with the observation that LY2109761 treatment resulted in decreased *THY1* expression and restored the sensitivity of recurrent tumors to TMZ/IR (Figs. 4A and 4B respectively), prompted us to investigate *THY1* further. In human cancers, *THY1* is associated with a poor prognosis, is linked with cancer stem cells and plays a role in invasion, metastasis, immune evasion, and epithelial to mesenchymal transition(*16-18*). Given the association of *THY1* with treatment resistance and a mesenchymal signature, its notable upregulation within the recurrent tumor samples, and its status as a cell surface marker, we quantitatively evaluated the presence of THY1+ cells in treatment-naïve tumor biopsies and observed that THY1+ cells constituted 6-10% of the population. In contrast, 75-96% of the cells within recurrent tumors were found to be THY1+ (Figs. 5A,B). FACS isolation and expansion of THY1+ cells from pre-treatment samples (Pre-THY1+), confirmed that they retained the expression of cell surface THY1(Figs. 5C,D). Pre-THY1+ cells were then implanted intracranially into nude mice and treated with TMZ/IR. These experiments revealed that the Pre-THY1+ cells were in fact inherently treatment resistant to a degree that mirrored the recurrent tumors (Fig. 5E). Additionally, the survival of mice bearing intracranial tumors derived using Pre-THY1+ cells was similar to mice having tumors derived from recurrent cells (Fig. 5F). This finding, combined with the consistent observation that each of the recurrent tumors (R1-R4, Fig 5A) exhibited an enrichment of THY1+ cells when compared to their respective pre-treatment biopsy (P1-P3, Fig. 5A) suggests that THY1+ cells represented a treatment recalcitrant cell population within the treatment-naïve samples, have features of a stem cell and mesenchymal phenotype, and may be responsible for tumor recurrence due to tumor repopulation.

To assess the clinical significance of upregulated *THY1* and its association with treatment resistance, we analyzed paired human GBM specimens from the GLASS consortium and other

clinical databases which revealed that *THY1* gene expression is significantly upregulated in the majority of recurrent tumors (Figs. 5G,F; Fig. S4). We then analyzed the TCGA database and identified that high *THY1* expression was associated with significantly worse progression-free and overall survival (Figs. 5I,J). These findings illustrate that our model paralleled the clinical scenario, and further emphasize the role of *THY1* in the development of TMZ/IR resistance.

***THY1* expression in human GBM is spatial niche-dependent**

Our *in vivo* studies suggesting that *THY1* expression is associated with therapeutic resistance and a stem and mesenchymal gene expression signature, combined with recent studies suggesting that THY1+ cells often reside within a perivascular or stem cell niche and are associated with a mesenchymal and stem cell gene expression pattern (*17, 19*), prompted us to evaluate the spatial distribution of *THY1* expressing cells in patient-derived tumor tissue. Spatial quantitative whole transcriptome analyses (spatial transcriptomics) of image-guided intraoperative human GBM biopsies from a region of high perfusion(vascularity) revealed that *THY1* expression significantly co-localized within the perivascular niche, characterized by co-expression of a glioma stem cell and mesenchymal signature, as well as TGFβ signaling (Fig. 6; Fig. S5A). We also performed spatial transcriptomics on a biopsy derived from a low perfusion region. This analysis also revealed that *THY1* was expressed within the perivascular niche, and was significantly co-localized with a mesenchymal and stem cell signature with upregulation of TGFβ signaling (Figs. 6D, F; Fig. S5B).

Since tumor-associated macrophages are known to drive malignant growth, stem cell maintenance, and epithelial to mesenchymal transition (EMT) (*3, 20-23*), we analyzed our spatial transcriptomic data which revealed that *THY1* also consistently co-localized with a macrophage gene expression profile (Fig. S5). We then performed gene ontology pathway enrichment

analyses for THY1 high vs low regions which revealed that cell adhesion and extracellular matrix pathways are highly upregulated in THY1-enriched regions both in the hypervascular(Fig. S6A,C) and hypovascular(Figs. S6B, D) samples, supporting our *in vivo* analyses (Fig. 2C). These data show that THY1+ cells consistently localize within a common niche, suggesting a critical role within the tumor microenvironment in a signaling axis that contributes to maintenance of a mesenchymal and cancer stem cell phenotype which contributes to treatment resistance.

**DISCUSSION**

Despite aggressive therapy for GBM with maximal safe resection and TMZ/IR, recurrence is inevitable, and therapeutically actionable mechanisms that drive resistance have yet to be identified. In an effort to characterize the molecular basis for the development of therapeutic resistance in GBM, we have analyzed a pre-clinical *in vivo* recurrence model along with spatial analyses of patient-derived biopsies. A key finding from the described studies indicates that a rare population of pre-existing, therapy-resistant tumor cells within the treatment-naïve GBM likely drive tumor recurrence. Specifically, this THY1+ cell population resides within a perivascular tumor niche strongly expressing EMT and stem cell signatures, and co-localizing with macrophages. Our findings also suggest that tumor recurrence may be driven through critical cell-cell interactions, possibly involving macrophages, within the perivascular tumor microenvironment that drive a mesenchymal transition.

The GBM recurrence model that we have developed recapitulates the clinical treatment paradigm and results in profoundly resistant tumors at recurrence. Most notable was the finding that THY1 expression was increased greater than 100-fold in recurrent biopsies compared to pre-treatment biopsies. We then isolated, using THY1 as a cell surface marker, a population of cells

from treatment-naïve tumors that recapitulated the treatment resistance phenotype of the recurrent tumor samples. The biological significance and clinical relevance of these results is further emphasized by the finding that THY1 expression is significantly upregulated in the majority of patients at the time of recurrence, and that increased THY1 expression was associated with worse PFS and OS. Although clonal selection of pre-existing therapy-resistant cells in GBM has been described previously(*8, 24-26*), the findings presented here provide a strong proof of the concept and identifies a specific phenotype and gene expression profile that characterizes this cell population.

Gene expression analysis of replicate paired pre-treatment and recurrent tumors from the same mouse revealed that development of a resistant phenotype was also associated with elevated expression of genes related to mesenchymal transition, stemness, cell adhesion and components of the extracellular matrix, as well as downregulation of genes associated with cell death. A mesenchymal gene expression signature results from the biological process of epithelial–mesenchymal transition (EMT) and is characterized by an enhanced capacity for invasion and metastasis in many malignancies (*6, 27-29*). THY1 is among the most significantly upregulated membrane proteins in cells acquiring a mesenchymal phenotype and cells with high expression of THY1 can possess stem cell properties(*15-18, 30, 31*). THY1 is a cell surface receptor that has been identified in several nonpathological cell types and is critical for cell-cell communication as well as cell-matrix interactions resulting in many physiological processes including proliferation, adhesion, and migration(*15, 30-32*). THY1 has been identified in a number of malignancies including renal cell cancers, breast cancer, hepatocellular carcinomas, ovarian cancer, and pancreatic tumors(*19, 31-36*) and has been associated with invasion, metastasis, immune evasion, and poor prognosis, all of which are hallmarks of EMT.

In our paired *in vivo* analyses, the recurrent samples which had THY1 upregulation also had significantly increased expression of genes associated with cell morphogenesis, cell-cell contact, as well as cell adhesion and extracellular structure organization. These results were corroborated by our gene ontology pathway enrichment analyses of human GBM specimens (Fig. S6). These cellular pathways mediate signals for growth, survival, differentiation, and resistance to cell death (*37, 38*). Avril *et al* demonstrated that THY1/CD90+ tumors have increased association with invasiveness and multi-focal tumor presentation, which further supports a role for THY1 in cell-cell communication and migration(*32*).

Therapeutic resistance in glioblastoma is driven by marked inter- and intra-tumoral heterogeneity both at the cellular and microenvironmental level(*3, 7, 39-41*). In the context of the tumor microenvironment (TME), distinct tumor niches, especially perivascular, hypoxic, and invasive tumor niches, have been shown to be enriched with therapy-resistant cancer stem cell populations (*3, 9, 40-43*). These niches support resistant populations and play a critical role in tumor recurrence, as the interplay between the treatment refractory cells and adjacent cells including immune, stromal, differentiated cancer, glial, neuronal, and endothelial cells drives quiescence, invasion, immune suppression as well as other features promoting treatment resistance(*3, 44-46*). In order to target these stem-like, therapy-resistant cells, the signaling cascades that promote a resistant phenotype in the context of the local TME need to be better understood. The recently developed technique of spatial transcriptomics (ST)(*47, 48*) provides the ability to interrogate whole transcriptome expression analysis *in situ*, permitting the assessment of the local tumor microenvironment. Due to the robust and reproducible evidence that THY1-positivity serves as a marker for a therapy resistant phenotype and hence may serve as a spatial landmark, we performed ST analyses of image-guided biopsies of a patient-derived

GBM. This analysis was performed in an unsupervised and spatially-naïve manner and gene expression data was then superimposed onto the original H+E imaging. We found that in the analyses of hyper-perfused and hypo-perfused regions of a single GBM, THY1 expression consistently co-localized with a mesenchymal and stem-like signature and was found primarily in the perivascular niche (*17*), validating our studies in mouse models. Furthermore, our ST studies revealed a co-localization of THY1 expression with a macrophage gene expression signature. Tumor-associated macrophages (TAMs) have been shown to maintain stem cell populations(*3, 20, 39, 49, 50*), and promote invasiveness and immune evasion through numerous interactions. For example, in breast cancer, TAMs were shown to preferentially infiltrate THY1+ regions, bind the THY1 receptor on cancer stem cells which resulted in juxtracrine signaling promoting invasiveness and supporting a stem cell niche, with activation of SRC and NFκB signaling cascades(*19*). These studies further revealed that depletion of macrophages resulted in arrest of tumor growth. In glioma, a recent study demonstrated that increased THY1 expression correlated with SRC phosphorylation, and resulted in a SRC-dependent tumor cell migration as well as cell-matrix interaction which was inhibited by the SRC-inhibitor, dasatinib(*32*). Interestingly, a recent study found that local THY1+ mesenchymal stem cells induced glioma progression through increasing tumor proliferation and cell migration(*18*). Our data, in conjunction with existing literature, highlight the importance of cell-cell interactions within the TME in tumor progression and the critical role of THY1 in paracrine/juxtracrine signaling within its local niche.

Our *in vivo* recurrent tumors displayed a mesenchymal gene expression profile characteristic of TGFβ pathway activation, which was further validated by ST analyses of our patient-derived tissues. A number of studies have independently demonstrated a role for TGFβ

signaling in treatment resistance (*51-55*), expression of stem cell markers, neurosphere formation ability as well as tumorigenic potential in mouse models (*54, 56, 57*). Furthermore, inhibition of TGFβ signaling has been associated with a depletion of the stem cell population in breast cancer, leukemia and glioblastoma(*56-60*). Our findings support this as inhibition of TGFβ signaling using LY2109761 decreased the expression of mesenchymal and stem-like genes. Furthermore, treatment of recurrent tumors with LY2109761 restored sensitivity to TMZ/IR. Importantly, although LY2109761 had minimal efficacy as single agent, a significant restoration in sensitivity to standard of care TMZ/IR when the two modalities were combined. This observation directly implicates the TGFβ signaling pathway in imparting a mesenchymal, stem-like, therapy-resistant phenotype as previously described(*60*). Recent clinical trials investigating various TGFβ inhibitors have not shown promise, but have typically utilized TGFβ inhibitors alone or in combination with other drugs including lomustine (*61, 62*). However, our findings suggest that TGFβ inhibition may be most effective in a recurrent setting to reverse the resistance to TMZ/IR, especially if patients are enriched for the expression of a mesenchymal and stem-like signature described here. The specific pathway to resistance likely only occurs in a subpopulation of patients as evidenced by Wang *et al* who found mutations in LTBP4, a known activator of the TGFβ pathway, in 11% of patients at recurrence (*8*). Therefore, identifying subgroups of patients who are likely to benefit from TGFβ targeting is critical(*53*). Activation of the TGFβ signaling pathway and a mesenchymal phenotype is also associated with enhanced capacity to repair DNA damage thereby leading to chemo- and radiation-resistance through a number of transcription factors (*63*). For example, ZEB2, which was upregulated in our recurrent samples, has been shown to affect ATM/ATR activity upon DNA damage (*64*). Its homolog ZEB1,

promotes radioresistance in breast cancer by regulating the stability of CHK1 and regulates TMZ sensitivity via regulation of MGMT in glioblastoma (*65, 66*).

The development of recurrence is a dynamic process that is poorly understood. Many have theorized that the evolutionary pressure during treatment results in selection of clonal cells versus expansion and mutation of a subclonal population of cells (*5, 24, 25, 67*). Our findings demonstrate that evolution and growth of a pre-existing tumor-cell sub-clonal population can also lead to recurrence. Chowell *et al*, demonstrated that treatment-naïve tumors often harbor rare treatment-resistant subclones which are undetectable with standard assays(*24*). A study by Kim *et al* found that the genetic path to tumor recurrence can be unique and difficult to predict when examined across multiple samples (*5*). Others have demonstrated that various subclones from a single tumor can exhibit variable treatment responses *in vitro*, and asserted that this information can be used to predict clinical response(*68*).

Although *in vivo* immunocompromised murine models do not perfectly replicate the clinical paradigm or the human tumor microenvironment, our findings are validated by clinical findings. Furthermore, our human spatial transcriptomic analyses provide additional insights into interactions between human tumor cells and the tumor microenvironment. The use of patient-derived explants rather than immortalized cell lines in an intracranial mouse model to evaluate the evolution of resistance to combination therapy using a genome wide analysis of gene expression also provides confidence that our findings approximate the clinical setting. Consistent with clinical experience, our results demonstrate that adjuvant TMZ prolonged the overall survival from 7 weeks to 13 weeks. The development of recurrence in animals while undergoing adjuvant TMZ suggests that the tumor were truly resistant. In addition, the demonstration that resistance to TMZ/IR was recapitulated upon re-implantation of recurrent tumor tissues confirms

this conclusion. Further efforts are needed to define how inherently resistant cells drive recurrence through interactions within the perivascular niche, which may lead to the identification of pathways to target for clinical benefit. In the recurrence model described here, we have utilized a combination of TMZ/IR to evaluate the mechanisms of treatment resistance. Although combination TMZ and IR is standard of care for GBM patients, a number of reports have tested the molecular basis for GBM resistance utilizing a single modality only (*69, 70*), which although important, does not mimic the emergence of resistance in a clinical settings.

## MATERIALS AND METHODS

### Patient-derived primary neurosphere culture

Low passage, patient-derived primary GBM neurosphere cells have been previously described (*71*), and were maintained in neurosphere medium composed of DMEM/F12 medium (#11320-033, Life Technologies, Carlsbad, CA) plus N2 supplement(#17502-048, Life Technologies, Carlsbad, CA), 0.5mg/ml BSA (#A4919, Sigma-Aldrich Co., St. Louis, MO), 25µg/ml Gentamicin (#15750-060, Life Technologies, Carlsbad, CA), 0.5% antibiotic/antimycotic (#15240-096, Life Technologies, Carlsbad, CA), 20ng/ml bFGF and 20 ng/ml EGF (#100-15 and #100-18B, PeproTech, Rocky Hill NJ). Cultures were derived from resected brain tumor specimens collected at Henry Ford Hospital (Detroit, MI) with written informed consent from patients, under a protocol approved by the Institutional Review Board.

### Intracranial Implantation

All research involving animals complied with protocols approved by the University Committee on Use and Care of Animals(Protocol # PRO00008583). Cultured neurosphere cells were dissociated and suspended in DMEM/F12 medium, and implanted intracranially into five-week-old athymic nude Foxn1nu mice (Harlan Laboratories, Indianapolis, IN). Mice were anesthetized

with a ketamine/xylazine (0.1/0.02mg/kg) mixture. The head surface was prepared with topical antiseptic solution (70% ethanol). A 1cm incision was made 2mm to the right of the midline and 1 mm retro-orbitally. The skull was exposed with a cotton-tip applicator and a handhold drill was used to drill a hole 1.5 mm anterior to bregma and 0.5 mm right to the midline. A 1µl cell suspension of $3x10^5$ cells was injected using a 30-gauge needle attached to a Hamilton syringe and a stereotactic fixation device (Stoelting, Wood Dale, IL) at a depth of 1.5 mm underneath the skull surface. The hole was covered using bonewax (#W810, Ethicon, Somerville, NJ) and the incision was sealed using Vetbond (#1469SB, Vetbond, 3M, Saint Paul, MN). 100 µl of carprofen was subcutaneously injected following the surgical procedure as pain reliever. Mice were monitored and retained in the study until they displayed any physical or neurological symptoms due to tumor burden.

**Subcutaneous Implantation**

Five-week-old athymic nude Foxn1nu mice were inoculated subcutaneously with $5 \times 10^6$ dissociated neurosphere cells into the flank on each side. Each injection contained a total volume of 200 µL cell suspension in 50% DMEM/F12 medium mixed with 50% BD Matrigel™ Basement Membrane Matrix (#356234, Becton, Dickinson and Company, East Rutherford, NJ). Caliper measurements were conducted weekly to determine tumor volumes using the formula $V = (\text{length}/2) \times (\text{width}^2)$.

**Magnetic resonance imaging (MRI)**

MRI scans were performed on a 9.4T, 16 cm horizontal bore (Agilent Technologies, Inc., Santa Clara, CA) Direct Drive system with a mouse surface receive coil (m2m Imaging, Corp., Cleveland, OH) actively decoupled to a whole-body volume transmit coil (Rapid MR International, LLC., Columbus, OH). 50ul of 0.5M gadolinium-DTPA (Magnevist; Bayer

Healthcare Pharmaceuticals, Montville, NJ) was injected intraperitoneally 5 minutes before the mouse was anesthetized with a 1-2% isoflurane/air mixture. During MRI, a heated air system (Air-Therm Heater, World Precision Instruments, Sarasota, FL) was used to maintain animal body temperature. T1-weighted images were acquired for each animal with the following parameters: repetition time/echo time = 510/15ms, field of view = 20 x 20mm$^2$, matrix size = 128 x 128, slice thickness = 0.5mm, 25 slices, and two averages. Mice were screened for tumor burden every week starting six weeks post intracranial implantation. Mice were randomized into different treatment groups when tumor sizes reached approximately 20-30 mm$^3$. Weekly MRI was continued during treatment. A continuous two-week increase in tumor volume while on treatment after an initial response was classified as recurrence.

**Tumor Volume Analysis**

Image reconstruction was completed by in-house software. Tumors were manually contoured along the enhancing rim of the tumors on the T1-weighted post-contrast images, from which tumor volume was calculated using in-house software running in MATLAB(MathWorks, Natick, MA, version 2016b). To determine tumor volume, tumor voxels were multiplied by the voxel volume.

**Stereotactic biopsy**

Coordinates for MRI-guided biopsy were determined by a fiducial markers attached to the whole-body volume transmit coil and VnmrJ software (Agilent Technologies, Inc., Santa Clara, CA)(*12*) (Fig. S1). The mouse was moved to a stereotactic station along with the whole-body volume transmit coil. A 1cm incision was made and the skull was exposed with cotton-tip applicators. After biopsy location was recovered using the fiducial markers, a burr hole was drilled and a 22GA x 3 7/8” needle (#54722, Inrad, Kentwood, MI) attached to a vacuum syringe

was inserted into the tumor. Biopsy tissues were dissociated and cultured in NMGF medium immediately and were expanded for three passages, to eliminate non-dividing cells derived from normal mouse brain. Holes were covered using bonewax and incisions were sealed using Vetbond. 100ul of carprofen was subcutaneously injected following the surgical procedure.

**Treatment**

For mice bearing intracranial tumors, animals were randomized into treatment groups once their tumor volume reached 20-30mm$^3$ by MRI evaluation(Fig. 1). Temozolomide (LKT Laboratories, St Paul, MN) was suspended in Ora-Plus suspending vehicle (#0574-0303-16, Rotterdam, Netherlands) and administered to animals (66mg/kg) via oral gavage daily for five days per week. Cranial irradiation was carried out one hour post temozolomide treatment. Mice were restrained in a home-made plastic restraining device. A lead shield was used so that only the head was exposed to radiation using a Kimtron INC-320 orthovoltage irradiator (Kimtron Medical, Oxford, CT). A total of 20Gy radiation was delivered to each animal at 2 Gy/day for ten days. Maintenance temozolomide was delivered orally three times week every other week from the third week till animals became moribund. For mice with subcutaneous flank tumors, animals were randomized into study groups when subcutaneous tumors reached an approximate volume of 300 mm$^3$. Temozolomide and radiation were delivered via similar administration routes and treatment schedules as described above. Radiation was targeted at local tumor sites with a lead shield. LY2109761(50mg/kg) (AbMole, Houston, TX), a TGFβRI inhibitor, was reconstituted using Ora-Plus suspending vehicle and delivered to animals twice per day for five days every week for two weeks. For animals treated with temozolomide, LY2109761 and radiation, LY2109761 was administered one hour before radiation along with TMZ and six hours after radiation treatment.

**RNA sequencing and data analysis**

Pre-treatment and treatment tumor biopsies were collected and cultured in NMGF medium for 3 passages. Neurosphere cells ($1x10^5$) were used for RNA extraction. Total RNA was extracted using TRIzol (#10296010, Life Technologies, Carlsbad, CA) and ethanol precipitated per manufacturer's instructions. RNAseq library preparation and sequencing were completed by the DNA sequencing core at the University of Michigan. Specifically, 30~45 million 50nt-single-end reads were obtained from each sample with an estimated 20~30x sequencing depth. Sequencing reads were aligned to a human reference genome (hg19) using Tophat 2.0 and the transciptome was assembled by cufflinks 2.1.1 (*72, 73*). Differential expression analysis was performed using the EdgeR 3.0 package in R 3.0.3 (*74-77*). Genes with FDR < 0.05 were chosen for further pathway enrichment analysis using David Bioinformatics Resources program and GENEmania (*78-80*).

**Western Blot**

Cells were lysed with NP-40 lysis buffer (1% NP40, 150 mmol/L NaCl, and 25 mmol/L Tris, pH 8.0) supplemented with protease inhibitors (#11697498001, Complete Protease Inhibitor Cocktail, Roche, Basel, Switzerland) and phosphatase inhibitors (#04906845001, PhosSTOP, Roche, Basel, Switzerland). Concentration of protein was determined using DC Protein Assay Kit II (#500-0112, Bio-Rad, Hercules, CA). Equal amount of protein was loaded in each lane and resolved by 4% to 12% gradient or 10% NuPAGE Bis-Tris gels (#NP0322BOX, #WG1202BOX, Life Technologies, Carlsbad, CA). Proteins were transferred to 0.2-µm nitrocellulose membrane (#162-0112, Bio-Rad, Hercules, CA Membranes were incubated overnight at 4°C with primary antibodies after blocking, followed by incubation with appropriate horseradish peroxidase (HRP)–conjugated secondary antibody at room temperature for 1 hour. Amersham ECL Prime

Western Blotting Detection Reagent (#RPN2236, GE Healthcare&Life Sciences, Fairfield, CT) was used to detect the activity of peroxidase according to the manufacturer's protocol. Antibodies raised against Cdk6, Thy1, Sox2, Gli2 were purchased from Cell Signaling Technology (#3136, #9798, #2748, #2585, Beverly, MA). ZEB2 antibody was purchased from Santa Cruz (#sc-48789, Dallas, Texas) and VCAN, GAPDH-HRP conjugated antibodies were purchased from Abcam (#ab19345, #ab9385 Cambridge, England).

**qRT-PCR**

Total RNA from neurosphere cells was extracted as described in RNA sequencing session. 2.5ug RNA was subjected to reverse transcription using SuperScript® III First-Strand Synthesis System (#18080-051, Life Technologies, Carlsbad, CA). qPCR was performed, with three replicates, using the SYBR Premix Ex Taq II (Tli RNase H Plus)(# RR820L, Clontech, Mountain View, CA) and Mastercycler ep realplex$^2$ (Eppendorf, Hamburg, Germany). The qPCR program comprised 95°C for 60s and 40 cycles of 95°C for 5s, 60°C for 30s. Relative mRNA expression was calculated based on Comparative C Method (ΔΔC Method) embedded in the Eppendorf Realplex software. The list of primers is included in supplemental table 1.

**FACS and Flow Cytometry**

Cells were prepared utilizing standard protocols and suspended in 2% IFS/PBS. Cells were sorted Cells were sorted on BD FACSAria III #3 Cell Sorter and analyzed using BD FACSDiva Software (BD Biosciences). Antibodies used were anti-CD90 (BD Biosciences no. 559869), anti-CD133 PE (BD Biosciences 566593).

**Spatial transcriptomics**

Under an institutional review board approved study, intraoperative brain tumor specimens were collected at the University of Michigan using MRI-imaged guidance technology to localize specimen within contrast-enhanced tissue with low and high perfusion parameters. This research was in full compliance of all pertinent ethical regulations for research with human biospecimens and all data were de-identified (IRB HUM00175135). Human samples acquired were immediately frozen in liquid nitrogen/isopentane, after which they were imbedded in optimal cutting temperature compound and frozen. Tissue was sectioned onto Visium Spatial Gene Expression Slide(10X Genomics) and permeabilized to release mRNA to bind to spatially barcoded capture probes. This was used to synthesize cDNA followed by preparation of sequencing libraries and sequencing. Sequencing data was visualized using and the resulting images put together with Vslide (v1.1.115, MetaSystems GmbH). Sample data are imaged and analyzed with 10X genomics software(Space Ranger and Loupe Browser). The SpaceRanger output files were imported into R using the Load10x_Spatial function. Library size normalization for the spots was performed using the SCTransform function(*81*), controlling for the percent of mitochondrial genes expressed at each spot. We imputed gene counts using MAGIC to smooth out the data prior to performing dimension reduction using PCA and UMAP(*82*). Specifically, the principal components were computed using top variable genes after imputation, and embedding of data on the first 30 principal components is used for identifying clusters and learning UMAP embedding. Pathway enrichment scores for specific genesets are computed similar to Neftel *et al*(*83*). A geneset collection object was prepared by collating specific genesets of interest from MSigDb as well as other datasets(*84, 85*). Enrichment scores were computed based on the MAGIC-imputed counts data. All genes were grouped into 30 bins based

on mean expression. Within each given gene set, mean expression of each gene was computed along with one hundred other randomly sampled genes from the corresponding bins as target genes. The difference in mean expression of target genes of interest versus control genes was calculated at each spot to compute the enrichment scores. After enrichment scores for the genesets at each spot are calculated, we then generated scatterplots of pathway scores versus *THY1* expression, and computed Spearman partial correlations between the two controlling for the G1.S cell cycle score at the spots, to account for variations in cell viability across the tissue section. To determine spatial overlap between *THY1* expression and pathway activity, we performed a regional Fisher's exact test for each spot. Based on *THY1* expression and pathway scores, we binarized the data into THY1-positive and pathway-positive at their 75th quantile. We then reviewed the k=25 nearest neighbors for every spot, and performed a Fisher's exact test to determine if there is significant overlap of the two features, i.e. if the pathway scores happen to be specifically enriched at THY1-positive regions. The Fisher test p-values are then overlaid onto each spot on the tissue slice to visualize regions that have significant overlaps in the two features.

**Statistics**

Results of *in vivo* volume data are shown as mean with standard error with 5 replicates performed for studies. Student's t-test (unpaired) and ANOVA was performed to assess statistical significance with $p<0.05$ considered significant. Survival analyses were performed utilizing Kaplan-Meier survival and statistical significance tested utilizing log-rank (Mantel-Cox) analyses with p-values as shown utilizing Graphpad Prism(9.0). Assessment of publicly accessible data from The Cancer Genome Atlas and Glass Consortium(*86*) was analyzed for gene sets of interest.

**Supplementary Materials**
Supplementary Materials and Methods

*Fig. S1.* Representative consecutive serial MR images from a single animal after image-guided stereotactic biopsy procedure.

*Fig. S2.* Unsupervised clustering analysis of RNAseq data revealed that replicate independent pre-treatment samples clustered together and independent replicate recurrent samples clustered together and are distinct from the pretreatment samples.

*Fig. S3.* Recurrent samples do not show any noteworthy copy number alterations.

*Fig. S4.* Analyses of publicly available clinical cohorts (Murat, Shulte, and vandenBoom) reveals that THY1 expression is significantly increased in recurrent GBM compared to primary GBM.

*Fig. S5.* Spatial transcriptional (ST) analyses of human GBM reveal that *THY1* significantly co-localizes with increased TGFβ pathway and macrophage gene expression signatures.

*Fig. S6.* Regions of interest with *THY1* gene expression show an enrichment of cell adhesion and extracellular gene expression signatures.

*Table S1.* Primers utilized for qRT-PCR.

**Acknowledgments:** Tumor specimens obtained from the University of Michigan were obtained through the CNS Tissue Biorepository (HUM00024610) and the Henry Ford brain tumor center. The results shown here are in part based upon data generated by the TCGA Research Network: https://www.cancer.gov/tcga, and the Glass Consortium (https://www.glass-consortium.org/). We would like to thank Steven Kronenberg for assistance with editing and illustration of figures. We would also like to thank Kait Verbal for her assistance in acquiring tumor samples through the CNS Tissue Biorepository. We would like to thank Dah-Luen Huang, Pavlina Zafirovska,

Susan Dagenais, Judy Opp, Ingrid Bergin, and Olivia Koues for assistance in processing our ST samples.

**Funding:**

Research reported in this publication was supported by National Institute of Health(NIH) grants P01-CA085878 and 5R01CA241764. Research was supported by the National Cancer Institute(NCI) of the NIH under award number P30CA046592. M.O. V.R., and A.R. were supported by National Cancer Institute (NCI) R37CA214955, a gift from Agilent technologies, a University of Michigan MIDAS PODS Grant, and a Research Scholar Grant from the American Cancer Society (RSG-16-005-01). WNA received support from the Congress of Neurological Surgeons Tumor fellowship and private donations.

References:


1. R. Stupp *et al.*, Effects of radiotherapy with concomitant and adjuvant temozolomide versus radiotherapy alone on survival in glioblastoma in a randomised phase III study: 5-year analysis of the EORTC-NCIC trial. *Lancet Oncol* **10**, 459-466 (2009).
2. R. Stupp *et al.*, Radiotherapy plus concomitant and adjuvant temozolomide for glioblastoma. *N Engl J Med* **352**, 987-996 (2005).
3. D. Hambardzumyan, G. Bergers, Glioblastoma: Defining Tumor Niches. *Trends Cancer* **1**, 252-265 (2015).
4. N. R. Parker *et al.*, Intratumoral heterogeneity identified at the epigenetic, genetic and transcriptional level in glioblastoma. *Sci Rep* **6**, 22477 (2016).
5. H. Kim *et al.*, Whole-genome and multisector exome sequencing of primary and post-treatment glioblastoma reveals patterns of tumor evolution. *Genome Res* **25**, 316-327 (2015).
6. R. G. W. Verhaak *et al.*, Integrated Genomic Analysis Identifies Clinically Relevant Subtypes of Glioblastoma Characterized by Abnormalities in PDGFRA, IDH1, EGFR, and NF1. *Cancer cell* **17**, 98-110 (2010).
7. S. Osuka, E. G. Van Meir, Overcoming therapeutic resistance in glioblastoma: the way forward. *The Journal of clinical investigation* **127**, 415-426 (2017).
8. J. Wang *et al.*, Clonal evolution of glioblastoma under therapy. *Nat Genet* **48**, 768-776 (2016).
9. J. D. Lathia, J. M. Heddleston, M. Venere, J. N. Rich, Deadly teamwork: neural cancer stem cells and the tumor microenvironment. *Cell stem cell* **8**, 482-485 (2011).
10. J. D. Lathia, S. C. Mack, E. E. Mulkearns-Hubert, C. L. Valentim, J. N. Rich, Cancer stem cells in glioblastoma. *Genes Dev* **29**, 1203-1217 (2015).
11. X. Lan *et al.*, Fate mapping of human glioblastoma reveals an invariant stem cell hierarchy. *Nature* **549**, 227-232 (2017).
12. S. Galban *et al.*, MRI-Guided Stereotactic Biopsy of Murine GBM for Spatiotemporal Molecular Genomic Assessment. *Tomography* **3**, 9-15 (2017).
13. A. Balbous *et al.*, A mesenchymal glioma stem cell profile is related to clinical outcome. *Oncogenesis* **3**, e91 (2014).
14. S. Lamouille, J. Xu, R. Derynck, Molecular mechanisms of epithelial-mesenchymal transition. *Nat Rev Mol Cell Biol* **15**, 178-196 (2014).
15. J. E. Bradley, G. Ramirez, J. S. Hagood, Roles and regulation of Thy-1, a context-dependent modulator of cell phenotype. *Biofactors* **35**, 258-265 (2009).
16. T. Shahar *et al.*, Percentage of mesenchymal stem cells in high-grade glioma tumor samples correlates with patient survival. *Neuro Oncol* **19**, 660-668 (2017).
17. J. He *et al.*, CD90 is identified as a candidate marker for cancer stem cells in primary high-grade gliomas using tissue microarrays. *Mol Cell Proteomics* **11**, M111 010744 (2012).
18. Q. Zhang *et al.*, CD90 determined two subpopulations of glioma-associated mesenchymal stem cells with different roles in tumour progression. *Cell Death Dis* **9**, 1101 (2018).
19. H. Lu *et al.*, A breast cancer stem cell niche supported by juxtacrine signalling from monocytes and macrophages. *Nature cell biology* **16**, 1105-1117 (2014).
20. D. Hambardzumyan, D. H. Gutmann, H. Kettenmann, The role of microglia and macrophages in glioma maintenance and progression. *Nat Neurosci* **19**, 20-27 (2016).
21. A. Wu *et al.*, Glioma cancer stem cells induce immunosuppressive macrophages/microglia. *Neuro Oncol* **12**, 1113-1125 (2010).
22. W. Zhou *et al.*, Periostin secreted by glioblastoma stem cells recruits M2 tumour-associated macrophages and promotes malignant growth. *Nature cell biology* **17**, 170-182 (2015).
23. E. Gangoso *et al.*, Glioblastomas acquire myeloid-affiliated transcriptional programs via epigenetic immunoediting to elicit immune evasion. *Cell* **184**, 2454-2470 e2426 (2021).
24. D. Chowell *et al.*, Modeling the Subclonal Evolution of Cancer Cell Populations. *Cancer Res* **78**, 830-839 (2018).
25. L. Ding *et al.*, Clonal evolution in relapsed acute myeloid leukaemia revealed by whole-genome sequencing. *Nature* **481**, 506-510 (2012).

26. T. Mazor *et al.*, DNA Methylation and Somatic Mutations Converge on the Cell Cycle and Define Similar Evolutionary Histories in Brain Tumors. *Cancer cell* **28**, 307-317 (2015).
27. K. P. Bhat *et al.*, Mesenchymal differentiation mediated by NF-kappaB promotes radiation resistance in glioblastoma. *Cancer cell* **24**, 331-346 (2013).
28. Y. Piao *et al.*, Acquired resistance to anti-VEGF therapy in glioblastoma is associated with a mesenchymal transition. *Clin Cancer Res* **19**, 4392-4403 (2013).
29. W. Y. Cheng, J. J. Kandel, D. J. Yamashiro, P. Canoll, D. Anastassiou, A multi-cancer mesenchymal transition gene expression signature is associated with prolonged time to recurrence in glioblastoma. *PloS one* **7**, e34705 (2012).
30. L. Leyton *et al.*, Thy-1/CD90 a Bidirectional and Lateral Signaling Scaffold. *Front Cell Dev Biol* **7**, 132 (2019).
31. C. Sauzay, K. Voutetakis, A. Chatziioannou, E. Chevet, T. Avril, CD90/Thy-1, a Cancer-Associated Cell Surface Signaling Molecule. *Front Cell Dev Biol* **7**, 66 (2019).
32. T. Avril *et al.*, CD90 Expression Controls Migration and Predicts Dasatinib Response in Glioblastoma. *Clin Cancer Res* **23**, 7360-7374 (2017).
33. B. Bussolati, S. Bruno, C. Grange, U. Ferrando, G. Camussi, Identification of a tumor-initiating stem cell population in human renal carcinomas. *FASEB J* **22**, 3696-3705 (2008).
34. L. Zhu, W. Zhang, J. Wang, R. Liu, Evidence of CD90+CXCR4+ cells as circulating tumor stem cells in hepatocellular carcinoma. *Tumour Biol* **36**, 5353-5360 (2015).
35. Z. F. Yang *et al.*, Significance of CD90+ cancer stem cells in human liver cancer. *Cancer cell* **13**, 153-166 (2008).
36. V. S. Donnenberg *et al.*, Localization of CD44 and CD90 positive cells to the invasive front of breast tumors. *Cytometry B Clin Cytom* **78**, 287-301 (2010).
37. R. Schmidmaier, P. Baumann, ANTI-ADHESION evolves to a promising therapeutic concept in oncology. *Current medicinal chemistry* **15**, 978-990 (2008).
38. R. Kalluri, R. A. Weinberg, The basics of epithelial-mesenchymal transition. *The Journal of clinical investigation* **119**, 1420-1428 (2009).
39. B. C. Prager, S. Bhargava, V. Mahadev, C. G. Hubert, J. N. Rich, Glioblastoma Stem Cells: Driving Resilience through Chaos. *Trends Cancer* **6**, 223-235 (2020).
40. S. Seidel *et al.*, A hypoxic niche regulates glioblastoma stem cells through hypoxia inducible factor 2 alpha. *Brain* **133**, 983-995 (2010).
41. D. L. Schonberg, D. Lubelski, T. E. Miller, J. N. Rich, Brain tumor stem cells: Molecular characteristics and their impact on therapy. *Mol Aspects Med* **39**, 82-101 (2014).
42. D. Schiffer, L. Annovazzi, C. Casalone, C. Corona, M. Mellai, Glioblastoma: Microenvironment and Niche Concept. *Cancers (Basel)* **11**, (2018).
43. J. D. Lathia *et al.*, Integrin alpha 6 regulates glioblastoma stem cells. *Cell stem cell* **6**, 421-432 (2010).
44. X. Wang *et al.*, Reciprocal Signaling between Glioblastoma Stem Cells and Differentiated Tumor Cells Promotes Malignant Progression. *Cell stem cell* **22**, 514-528 e515 (2018).
45. M. Jamal, B. H. Rath, E. S. Williams, K. Camphausen, P. J. Tofilon, Microenvironmental regulation of glioblastoma radioresponse. *Clin Cancer Res* **16**, 6049-6059 (2010).
46. M. Jamal, B. H. Rath, P. S. Tsang, K. Camphausen, P. J. Tofilon, The brain microenvironment preferentially enhances the radioresistance of CD133(+) glioblastoma stem-like cells. *Neoplasia* **14**, 150-158 (2012).
47. E. Berglund *et al.*, Spatial maps of prostate cancer transcriptomes reveal an unexplored landscape of heterogeneity. *Nat Commun* **9**, 2419 (2018).
48. S. Maniatis *et al.*, Spatiotemporal dynamics of molecular pathology in amyotrophic lateral sclerosis. *Science* **364**, 89-93 (2019).
49. X. Z. Ye *et al.*, Tumor-associated microglia/macrophages enhance the invasion of glioma stem-like cells via TGF-beta1 signaling pathway. *J Immunol* **189**, 444-453 (2012).
50. T. Hara *et al.*, Interactions between cancer cells and immune cells drive transitions to mesenchymal-like states in glioblastoma. *Cancer cell* **39**, 779-792 e711 (2021).
51. S. A. Mani *et al.*, The epithelial-mesenchymal transition generates cells with properties of stem cells. *Cell* **133**, 704-715 (2008).
52. K. Polyak, R. A. Weinberg, Transitions between epithelial and mesenchymal states: acquisition of malignant and stem cell traits. *Nat Rev Cancer* **9**, 265-273 (2009).

53. N. S. Bayin *et al.*, Patient-Specific Screening Using High-Grade Glioma Explants to Determine Potential Radiosensitization by a TGF-beta Small Molecule Inhibitor. *Neoplasia* **18**, 795-805 (2016).
54. M. E. Hardee *et al.*, Resistance of glioblastoma-initiating cells to radiation mediated by the tumor microenvironment can be abolished by inhibiting transforming growth factor-beta. *Cancer Res* **72**, 4119-4129 (2012).
55. N. Oshimori, D. Oristian, E. Fuchs, TGF-beta promotes heterogeneity and drug resistance in squamous cell carcinoma. *Cell* **160**, 963-976 (2015).
56. H. Ikushima *et al.*, Autocrine TGF-beta signaling maintains tumorigenicity of glioma-initiating cells through Sry-related HMG-box factors. *Cell stem cell* **5**, 504-514 (2009).
57. J. Anido *et al.*, TGF-beta Receptor Inhibitors Target the CD44(high)/Id1(high) Glioma-Initiating Cell Population in Human Glioblastoma. *Cancer cell* **18**, 655-668 (2010).
58. K. Naka *et al.*, TGF-beta-FOXO signalling maintains leukaemia-initiating cells in chronic myeloid leukaemia. *Nature* **463**, 676-680 (2010).
59. M. Shipitsin *et al.*, Molecular definition of breast tumor heterogeneity. *Cancer cell* **11**, 259-273 (2007).
60. M. Zhang *et al.*, Trimodal glioblastoma treatment consisting of concurrent radiotherapy, temozolomide, and the novel TGF-beta receptor I kinase inhibitor LY2109761. *Neoplasia* **13**, 537-549 (2011).
61. A. A. Brandes *et al.*, A Phase II randomized study of galunisertib monotherapy or galunisertib plus lomustine compared with lomustine monotherapy in patients with recurrent glioblastoma. *Neuro Oncol* **18**, 1146-1156 (2016).
62. U. Bogdahn *et al.*, Targeted therapy for high-grade glioma with the TGF-beta2 inhibitor trabedersen: results of a randomized and controlled phase IIb study. *Neuro Oncol* **13**, 132-142 (2011).
63. M. H. Barcellos-Hoff, F. A. Cucinotta, New tricks for an old fox: impact of TGFbeta on the DNA damage response and genomic stability. *Sci Signal* **7**, re5 (2014).
64. A. E. Sayan *et al.*, SIP1 protein protects cells from DNA damage-induced apoptosis and has independent prognostic value in bladder cancer. *Proceedings of the National Academy of Sciences of the United States of America* **106**, 14884-14889 (2009).
65. P. Zhang *et al.*, ATM-mediated stabilization of ZEB1 promotes DNA damage response and radioresistance through CHK1. *Nature cell biology* **16**, 864-875 (2014).
66. F. A. Siebzehnrubl *et al.*, The ZEB1 pathway links glioblastoma initiation, invasion and chemoresistance. *Embo Mol Med* **5**, 1196-1212 (2013).
67. M. R. Blomquist *et al.*, Temporospatial genomic profiling in glioblastoma identifies commonly altered core pathways underlying tumor progression. *Neurooncol Adv* **2**, vdaa078 (2020).
68. R. Reinartz *et al.*, Functional Subclone Profiling for Prediction of Treatment-Induced Intratumor Population Shifts and Discovery of Rational Drug Combinations in Human Glioblastoma. *Clin Cancer Res* **23**, 562-574 (2017).
69. G. J. Kitange *et al.*, Inhibition of histone deacetylation potentiates the evolution of acquired temozolomide resistance linked to MGMT upregulation in glioblastoma xenografts. *Clin Cancer Res* **18**, 4070-4079 (2012).
70. T. C. Johannessen, R. Bjerkvig, Molecular mechanisms of temozolomide resistance in glioblastoma multiforme. *Expert review of anticancer therapy* **12**, 635-642 (2012).
71. A. C. DeCarvalho *et al.*, Gliosarcoma Stem Cells Undergo Glial and Mesenchymal Differentiation In Vivo. *Stem Cells* **28**, 181-190 (2010).
72. C. Trapnell, L. Pachter, S. L. Salzberg, TopHat: discovering splice junctions with RNA-Seq. *Bioinformatics* **25**, 1105-1111 (2009).
73. C. Trapnell *et al.*, Transcript assembly and quantification by RNA-Seq reveals unannotated transcripts and isoform switching during cell differentiation. *Nat Biotechnol* **28**, 511-U174 (2010).
74. M. D. Robinson, D. J. McCarthy, G. K. Smyth, edgeR: a Bioconductor package for differential expression analysis of digital gene expression data. *Bioinformatics* **26**, 139-140 (2010).
75. M. D. Robinson, G. K. Smyth, Moderated statistical tests for assessing differences in tag abundance. *Bioinformatics* **23**, 2881-2887 (2007).
76. M. D. Robinson, G. K. Smyth, Small-sample estimation of negative binomial dispersion, with applications to SAGE data. *Biostatistics* **9**, 321-332 (2008).
77. X. B. Zhou, H. Lindsay, M. D. Robinson, Robustly detecting differential expression in RNA sequencing data using observation weights. *Nucleic Acids Res* **42**, (2014).
78. D. W. Huang, B. T. Sherman, R. A. Lempicki, Systematic and integrative analysis of large gene lists using DAVID bioinformatics resources. *Nat Protoc* **4**, 44-57 (2009).

79. D. W. Huang, B. T. Sherman, R. A. Lempicki, Bioinformatics enrichment tools: paths toward the comprehensive functional analysis of large gene lists. *Nucleic Acids Res* **37**, 1-13 (2009).
80. D. Warde-Farley *et al.*, The GeneMANIA prediction server: biological network integration for gene prioritization and predicting gene function. *Nucleic Acids Res* **38**, W214-W220 (2010).
81. C. Hafemeister, R. Satija, Normalization and variance stabilization of single-cell RNA-seq data using regularized negative binomial regression. *Genome Biol* **20**, 296 (2019).
82. D. van Dijk *et al.*, Recovering Gene Interactions from Single-Cell Data Using Data Diffusion. *Cell* **174**, 716-729 e727 (2018).
83. C. Neftel *et al.*, An Integrative Model of Cellular States, Plasticity, and Genetics for Glioblastoma. *Cell* **178**, 835-849 e821 (2019).
84. S. Darmanis *et al.*, Single-Cell RNA-Seq Analysis of Infiltrating Neoplastic Cells at the Migrating Front of Human Glioblastoma. *Cell Rep* **21**, 1399-1410 (2017).
85. S. Muller *et al.*, Single-cell profiling of human gliomas reveals macrophage ontogeny as a basis for regional differences in macrophage activation in the tumor microenvironment. *Genome Biol* **18**, 234 (2017).
86. G. Consortium, Glioma through the looking GLASS: molecular evolution of diffuse gliomas and the Glioma Longitudinal Analysis Consortium. *Neuro Oncol* **20**, 873-884 (2018).

Fig. 1.

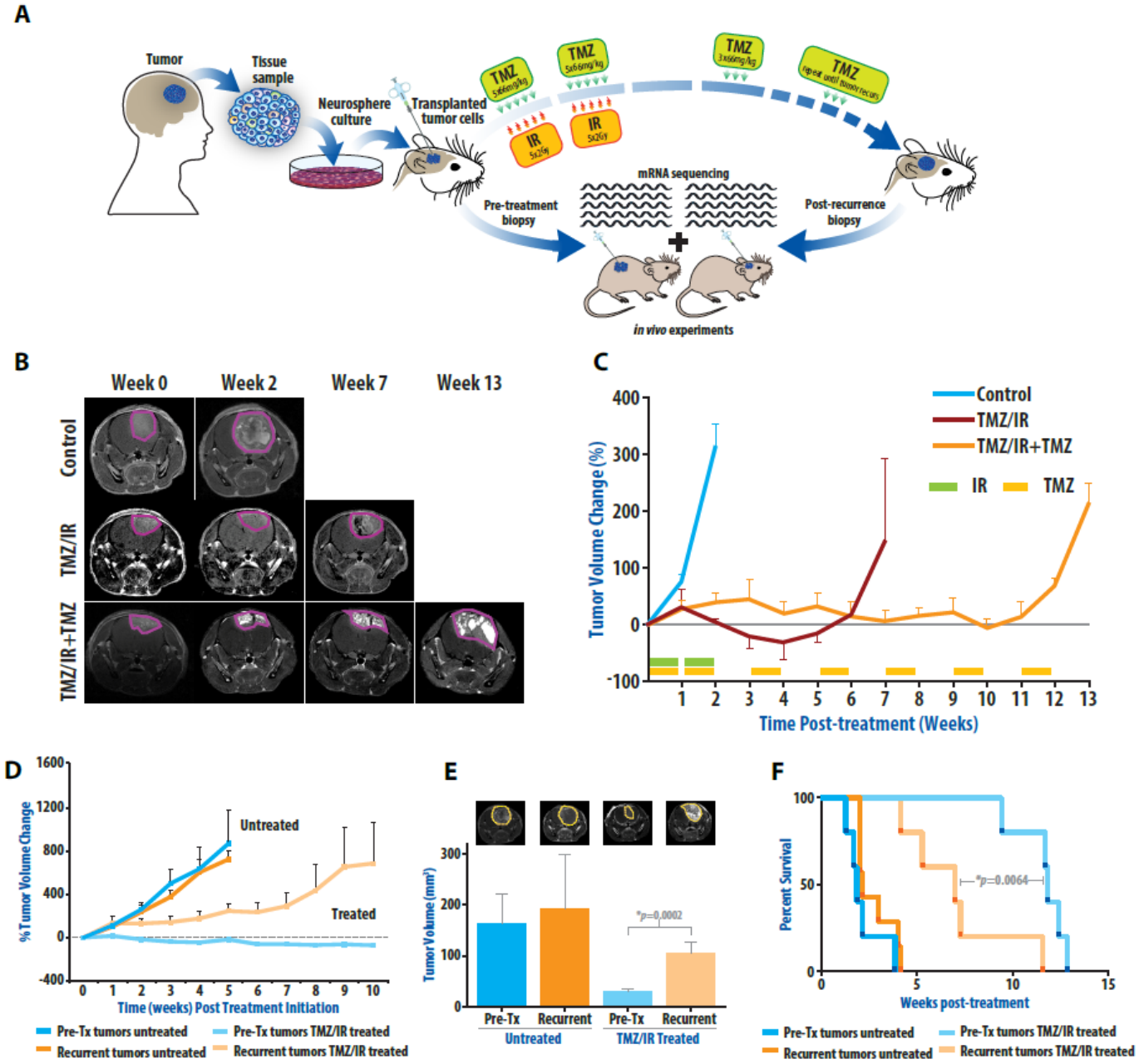
A
Tumor
Tissue sample
Neurosphere culture
Transplanted tumor cells
TMZ
IR
mRNA sequencing
Pre-treatment biopsy
Post-recurrence biopsy
in vivo experiments
B
Week 0
Week 2
Week 7
Week 13
Control
TMZ/IR
TMZ/IR+TMZ
C
Control
TMZ/IR
TMZ/IR+TMZ
IR
TMZ
Tumor Volume Change (%)
Time Post-treatment (Weeks)
D
Untreated
Treated
% Tumor Volume Change
Time (weeks) Post Treatment Initiation
Pre-Tx tumors untreated
Pre-Tx tumors TMZ/IR treated
Recurrent tumors untreated
Recurrent tumors TMZ/IR treated
E
Tumor Volume (mm³)
*p=0.0002
Pre-Tx
Recurrent
Untreated
TMZ/IR Treated
F
Percent Survival
*p=0.0064
Weeks post-treatment
Pre-Tx tumors untreated
Pre-Tx tumors TMZ/IR treated
Recurrent tumors untreated
Recurrent tumors TMZ/IR treated

**Fig. 1**. **Analysis of longitudinal intracranial GBM samples, pre-treatment and at recurrence, reveals development of a therapeutic resistant phenotype. (A)** Schematic of experimental design. Mice bearing intracranial tumors derived from human GBM explants are treated with concomitant temozolomide (TMZ) and radiation (IR) for two weeks followed by adjuvant TMZ until animals became moribund. Tumor biopsies are obtained pre-treatment and at recurrence to provide samples for molecular analysis and additional *in vivo* and *in vitro* comparative studies. **(B)** Representative MR images from Control, TMZ/IR and TMZ/IR+TMZ treatment groups at 0, 2, 7 and 13 weeks post-initiation. **(C)** Treatment response quantified using MR-imaging derived tumor volume changes in Control, TMZ/IR and TMZ/IR+TMZ intracranial tumor bearing groups. TMZ/IR treatment involved 2 weeks of concomitant TMZ/IR, while mice receiving TMZ/IR+TMZ received the initial 2 week treatment followed by maintenance adjuvant TMZ every other week. Percent change in tumor volume is shown as mean change in a cohort of five animals with SEM. **(D)** Pre-treatment(Pre-Tx) and post-treatment(recurrent) biopsy samples were re-implanted subcutaneously into the flanks of mice to evaluate their sensitivity to treatment as described in methods. Pre-treatment and recurrent tumors show similar growth rates in the absence of treatment, while recurrent tumors exhibit an inherent resistance to TMZ/IR. **(E)** Samples described in D were also evaluated intracranially. Tumor volumes derived from pre-treatment and recurrent tumors with or without TMZ/IR are shown as mean tumor volumes (+SEM) as well as representative MR images three weeks after treatment initiation. **(F)** Kaplan-Meier survival curve of mice after intracranial implantation of pre-treatment and recurrent tumors with or without TMZ/IR treatment. Mice bearing recurrent tumors have significantly worse survival with treatment.

Fig. 2.

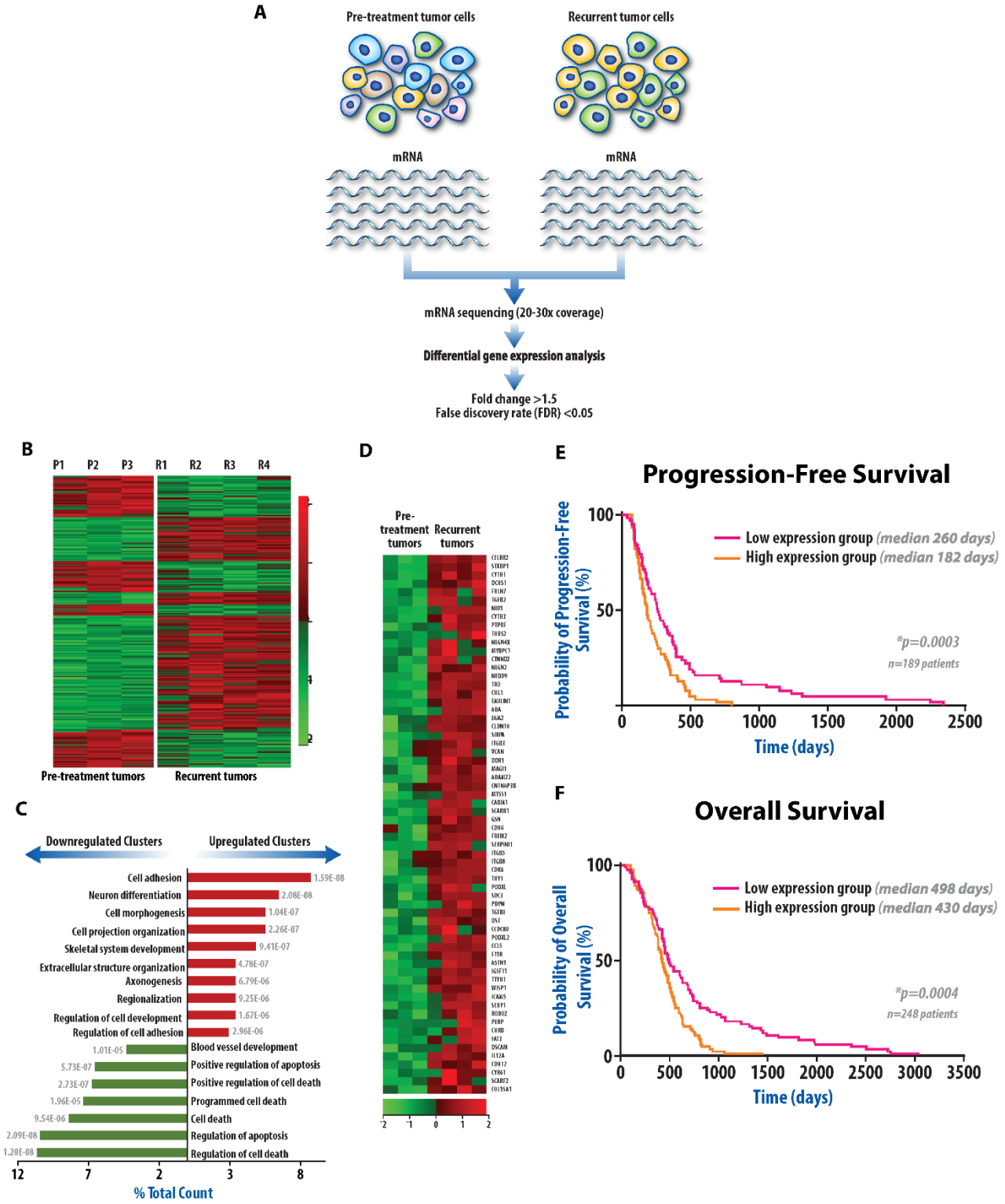
A
Pre-treatment tumor cells
Recurrent tumor cells
mRNA
mRNA
mRNA sequencing (20-30x coverage)
Differential gene expression analysis
Fold change >1.5
False discovery rate (FDR) <0.05
B
P1 P2 P3 R1 R2 R3 R4
Pre-treatment tumors
Recurrent tumors
C
Downregulated Clusters
Upregulated Clusters
Cell adhesion 1.59E-08
Neuron differentiation 2.08E-08
Cell morphogenesis 1.04E-07
Cell projection organization 2.26E-07
Skeletal system development 9.41E-07
Extracellular structure organization 4.78E-07
Axonogenesis 6.79E-06
Regionalization 9.25E-06
Regulation of cell development 1.67E-06
Regulation of cell adhesion 2.96E-06
1.01E-05 Blood vessel development
5.73E-07 Positive regulation of apoptosis
2.73E-07 Positive regulation of cell death
1.96E-05 Programmed cell death
9.54E-06 Cell death
2.09E-08 Regulation of apoptosis
1.20E-08 Regulation of cell death
12 7 2 3 8
% Total Count
D
Pre-treatment tumors
Recurrent tumors
-2 -1 0 1 2
E
Progression-Free Survival
Probability of Progression-Free Survival (%)
100
50
Low expression group (median 260 days)
High expression group (median 182 days)
*p=0.0003
n=189 patients
0 500 1000 1500 2000 2500
Time (days)
F
Overall Survival
Probability of Overall Survival (%)
100
50
0
Low expression group (median 498 days)
High expression group (median 430 days)
*p=0.0004
n=248 patients
0 500 1000 1500 2000 2500 3000 3500
Time (days)

**Fig. 2. RNAseq analyses reveal a resistant gene expression profile that predicts outcomes in clinical datasets. (A)** A diagrammatic representation of the experimental workflow. Paired pre-treatment and recurrent tumor samples are evaluated by next generation sequencing of RNA samples extracted from cells. **(B)** Unsupervised clustering analysis revealed that replicate independent pre-treatment samples clustered together had a similar gene expression pattern. Similarly independent replicate recurrent samples clustered together. Heatmap of differentially expressed genes in independent pre-treatment biopsies (P1,P2,P3) and recurrent tumor biopsies (R1,R2,R3,R4). **(C)** Functional clusters of upregulated and downregulated genes in recurrent tumors. Bar graph shows percentage of gene counts of each cluster compared to total upregulated or downregulated genes. P-value of each cluster is labeled next to each bar. Cell adhesion genes were upregulated in recurrent tumors. **(D)** Heatmap of individual genes within the highest upregulated clusters. Progression-free **(E)** and overall survival **(F)** and progression-free survival of GBM patients with high and low expression levels of a signature characterized by cell adhesion genes, showing that this upregulated signature predicts outcomes in GBM patients.

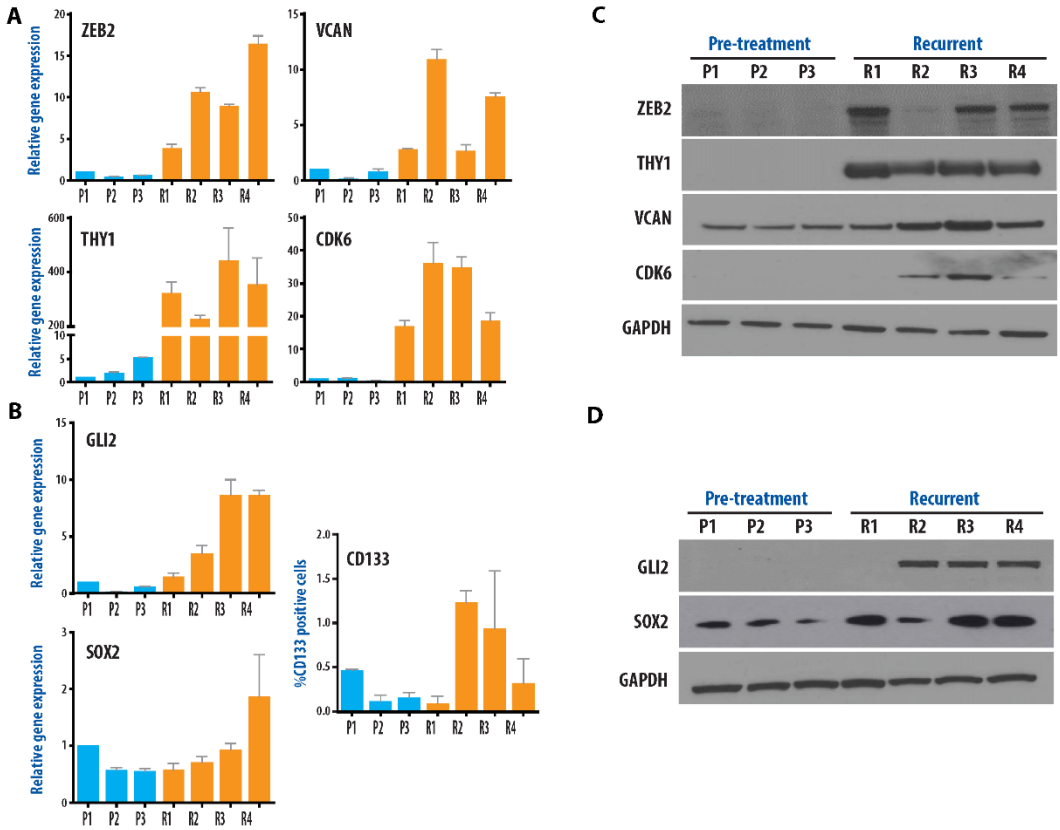
A
ZEB2
VCAN
THY1
CDK6
Relative gene expression
P1 P2 P3 R1 R2 R3 R4
B
GLI2
SOX2
CD133
%CD133 positive cells
C
Pre-treatment
Recurrent
ZEB2
THY1
VCAN
CDK6
GAPDH
D
GLI2
SOX2
GAPDH

Fig. 3.

**Fig. 3. Analyses of paired samples reveals development of a therapeutic resistant phenotype with a mesenchymal, and stem cell gene expression pattern. (A)** Upregulated genes in recurrent samples (R1-R4) associated with a mesenchymal signature were confirmed by qRTPCR, show notable upregulation in recurrent samples compared to pre-treatment samples (P1-P3). THY1 is most prominently differentially upregulated, greater than 100-fold compared to pre-treatment levels. **(B)** Upregulated genes in recurrent samples associated with a stem cell phenotype were confirmed using qRTPCR. FACS analysis of CD133 expression in pre-treatment and recurrent neurosphere cells (bottom right panel) shows upregulation of CD133+ cells in 3 of 4 samples at recurrence. **(C, D)** Western blot analysis confirmed that the protein levels for each of these genes were also increased in a majority of recurrent samples compared to their untreated counterparts.

Fig. 4.

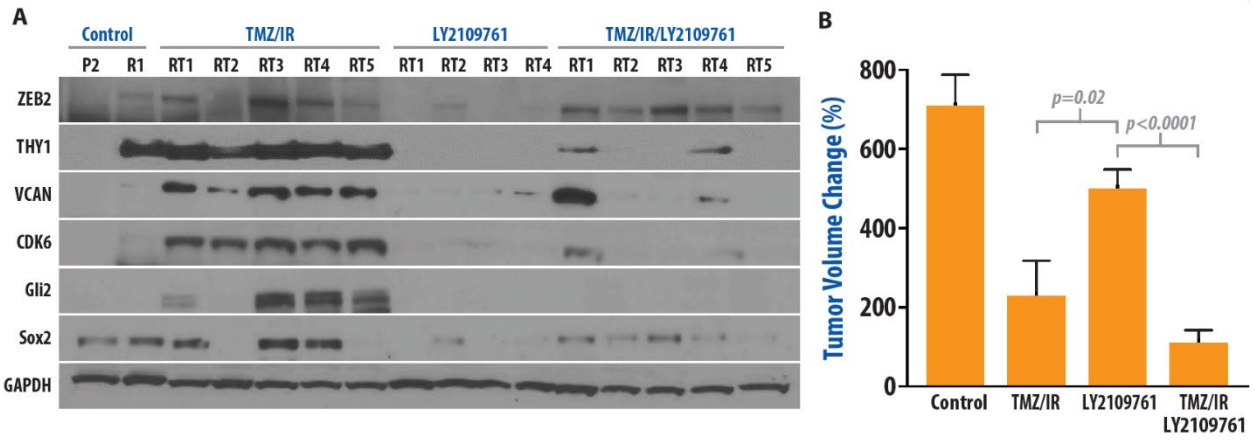


**Fig. 4. Inhibition of TGFβ signaling downregulates expression of mesenchymal and stem-like genes in recurrent tumors. (A)** Western blot analysis shows that inhibition of TGFβ signaling results in a marked decrease in expression of proteins associated with a mesenchymal and stem cell signature in recurrent tumor samples. P2 (treatment naïve sample 2). R1 (recurrent sample 1), RT1-RT5 (recurrent samples treated as indicated in five independent animals) with TMZ/IR, LY2109761, or combination of TMZ/IR and LY2109761 as described below. **(B)** Animals bearing flank pre-treatment tumors as well as recurrent tumors were randomized into four groups 1)An untreated group (control), 2)Treatment with TMZ (TMZ, 5 days/week at 66mg/kg) and IR (5 days/ week at 2Gy) for two weeks followed by TMZ (3 days/week at 66mg/kg) every other week (TMZ/IR), 3)Treatment with LY2109761 where mice received 50mg/kg LY2109761 twice every day, 5 days/week for the first two weeks followed by 3 days/week every other week (LY2109761), and 4)TMZ/IR/LY2109761 group where the animals were treated with a combination of the three aforementioned treatment modalities. 5 replicates animals were evaluated. Mean volume + SEM shown.

Fig. 5.

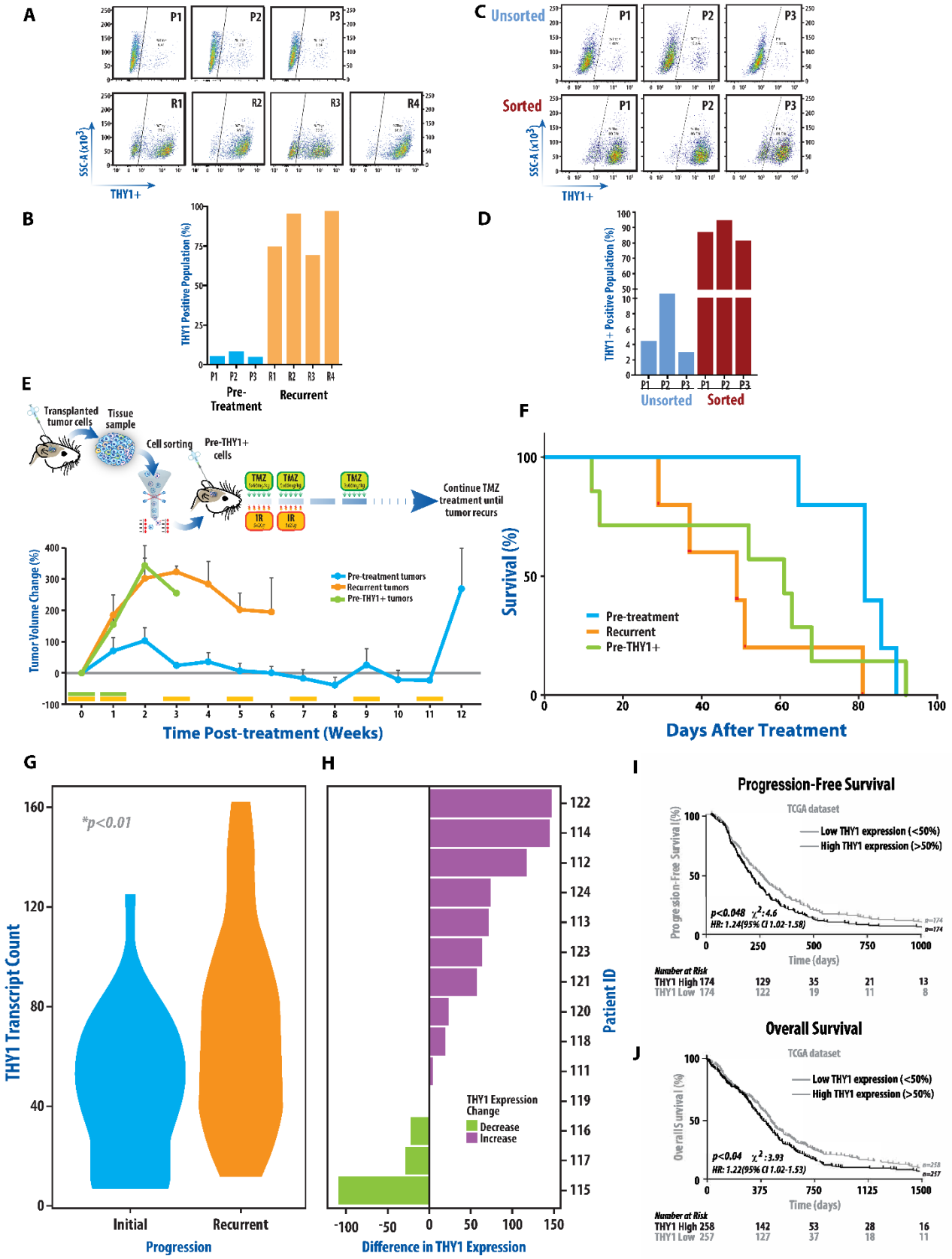
A
P1
P2
P3
R1
R2
R3
R4
SSC-A (x10³)
THY1+
B
THY1 Positive Population (%)
Pre-Treatment
Recurrent
C
Unsorted
Sorted
D
THY1+ Positive Population (%)
Unsorted
Sorted
E
Transplanted tumor cells
Tissue sample
Cell sorting
Pre-THY1+ cells
TMZ
IR
Continue TMZ treatment until tumor recurs
Tumor Volume Change (%)
Pre-treatment tumors
Recurrent tumors
Pre-THY1+ tumors
Time Post-treatment (Weeks)
F
Survival (%)
Pre-treatment
Recurrent
Pre-THY1+
Days After Treatment
G
*p<0.01
THY1 Transcript Count
Initial
Recurrent
Progression
H
Patient ID
THY1 Expression Change
Decrease
Increase
Difference in THY1 Expression
I
Progression-Free Survival
TCGA dataset
Low THY1 expression (<50%)
High THY1 expression (>50%)
Progression-Free Survival (%)
p<0.048 χ²: 4.6
HR: 1.24(95% CI 1.02-1.58)
Time (days)
Number at Risk
THY1 High 174 129 35 21 13
THY1 Low 174 122 19 11 8
J
Overall Survival
TCGA dataset
Low THY1 expression (<50%)
High THY1 expression (>50%)
Overall Survival (%)
p<0.04 χ²: 3.93
HR: 1.22(95% CI 1.02-1.53)
Time (days)
Number at Risk
THY1 High 258 142 53 28 16
THY1 Low 257 127 37 18 11

**Fig. 5. Rare THY1+ cell populations are identified in the pre-treatment samples, are inherently treatment resistant, and repopulate the recurrent tumors. (A)** THY1 cell positivity is highly upregulated in recurrent samples as seen by flow cytometry and representative bar graph **(B)**. 6-10% of pre-treatment samples (P1-P3) demonstrate THY1-positivity while 72-96% of recurrent samples (R1-R4) reveal THY1-positivity(left) with quantification of replicate experiments shown(right). **(C, D)** THY1-positive cells were immuno-purified from P1, P2 and P3 samples by FACS. This sorted THY1+ cell population was cultured for expansion and re-tested to confirm stable THY1 cell surface staining. **(E)** Sorted THY1+ cell population from P2 (Pre-THY1+) was implanted intracranially to assess treatment response. Resistance to TMZ/IR was observed in the Pre-THY1+ tumor bearing animals that mirrored the phenotype observed in recurrent tumors, but distinct from pre-treatment samples. Mean tumor volume (**E**) (+SEM) and survival analysis by Kaplan-Meier (**F**) are shown. **(G)** Analysis of longitudinal GBM specimens reveals significant upregulation of *THY1* expression in recurrent tumors(GLASS consortium) with most patients showing increased expression **(H)**. Evaluation of TCGA clinical database reveals *THY1* expression is associated with significantly worse recurrence-free **(I)** and overall survival **(J)**.

Fig. 6.

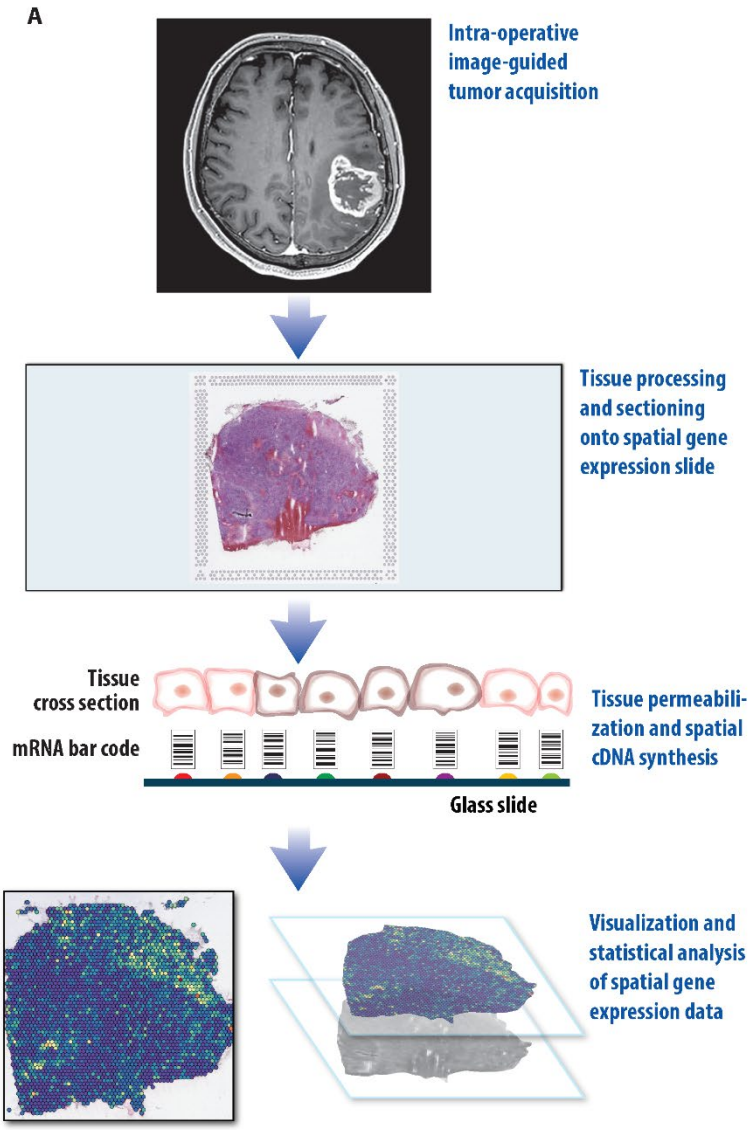
A
Intra-operative image-guided tumor acquisition
Tissue processing and sectioning onto spatial gene expression slide
Tissue cross section
mRNA bar code
Glass slide
Tissue permeabili-zation and spatial cDNA synthesis
Visualization and statistical analysis of spatial gene expression data

Fig. 6.

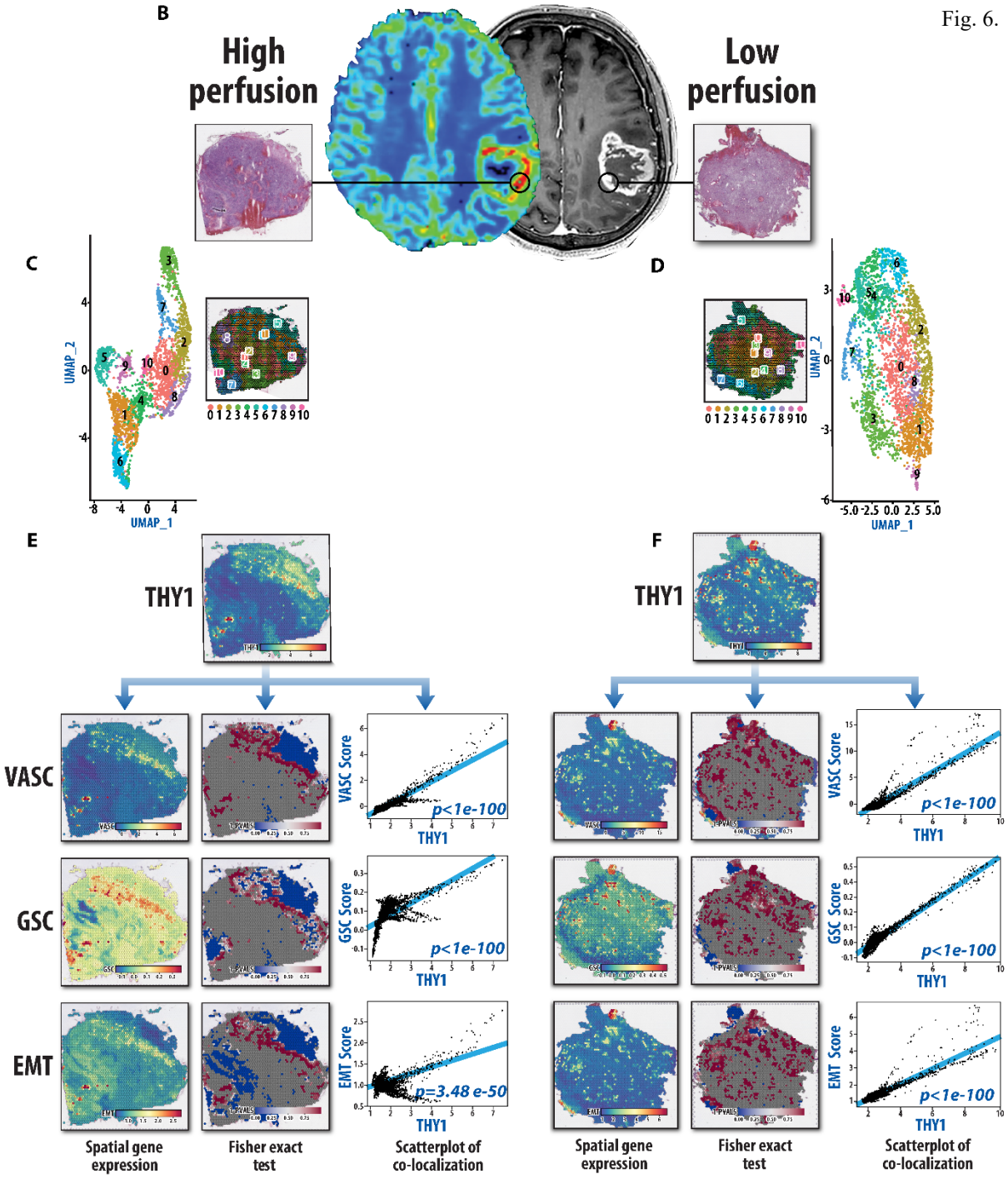
B
High perfusion
Low perfusion
C
D
UMAP_1
UMAP_2
0 1 2 3 4 5 6 7 8 9 10
E
F
THY1
VASC
GSC
EMT
VASC Score
GSC Score
EMT Score
p<1e-100
p=3.48 e-50
Spatial gene expression
Fisher exact test
Scatterplot of co-localization

**Fig. 6. Spatial transcriptomic analysis (ST) of treatment-naive human GBM biopsies reveal that *THY1* expression significantly co-localizes with a glioma stem cell (GSC), and epithelial to mesenchymal transition (EMT) gene expression signatures within the perivascular niche. (A)** A schematic depicting the experimental approach for evaluating the spatial distribution of gene expression profiles within a GBM biopsy. (**B**) MRI from a patient with primary GBM showing T1-post contrast weighted MRI and corresponding perfusion (CBV) scan. Two image-guided stereotactic biopsies were acquired, one from a contrast-enhancing region with relative high-perfusion, and a second from an enhancing region with low-perfusion. **(C,D)** UMAP analyses depicting spatial regions with unique gene expression profiles within both samples. **(E,F)** ST analysis of a GBM biopsy from a region with high perfusion **(E)** and Low Perfusion **(F)**. Spatial distribution of *THY1* expression is shown along with vascular (VASC), GSC, and EMT pathway enrichment scores. The left panels show the spatial gene expression of each individual gene set. The middle panel shows 1 minus p-values from a spatially local Fisher's exact test within each spot for significant overlap between regions with high pathway enrichment scores and high THY1 expression. Significance in spatial overlap between the pathway enrichment scores and *THY1* expression was tested by using a sliding window approach to perform spatially-local Fisher's test. On the right are scatterplots showing gene expression of *THY1*(x-axis) and enrichment scores for gene set of interest(y-axis) within each spatial location with line fitted. P-values show significance of correlation. *THY1* significantly co-localizes with these gene sets both in the high and low perfusion samples.